

Control of the transition frequency of a superconducting flux qubit by longitudinal coupling to the photon number degree of freedom in a resonator

Hiraku Toida^{1,*}, Takuya Ohrai,^{1,2} Yuichiro Matsuzaki,^{1,†} Kosuke Kakuyanagi,¹ and Shiro Saito^{1,2}

¹*NTT Basic Research Laboratories, NTT Corporation, 3-1 Morinosato-Wakamiya, Atsugi, Kanagawa 243-0198, Japan*

²*Department of Applied Physics, Faculty of Science, Tokyo University of Science, 6-3-1 Niijuku, Katsushika, Tokyo 125-8585, Japan*



(Received 13 May 2020; revised 16 August 2020; accepted 17 August 2020; published 3 September 2020)

We control the transition frequency of a superconducting flux qubit coupled to a frequency-tunable resonator comprising a direct current superconducting quantum interference device (dc SQUID) by microwave driving. The dc SQUID mediates the coupling between microwave photons in the resonator and a flux qubit. The polarity of the frequency shift depends on the sign of the flux bias for the qubit and can be both positive and negative. The absolute value of the frequency shift becomes larger by increasing the photon number in the resonator. These behaviors are reproduced by a model considering the magnetic interaction between the flux qubit and dc SQUID. The tuning range of the transition frequency of the flux qubit reaches ≈ 1.9 GHz. The effect of photon number fluctuation in the resonator to the dephasing rate of the flux qubit is also discussed.

DOI: [10.1103/PhysRevB.102.094502](https://doi.org/10.1103/PhysRevB.102.094502)

I. INTRODUCTION

Implementing a large-scale quantum system requires controllable qubits with excellent coherence properties. A superconducting qubit is one of the most promising candidates for implementing such a system with solid-state devices [1–4]. The transition frequency of a superconducting qubit is commonly controlled by applying magnetic flux to the superconducting loop of a direct current superconducting quantum interference device (dc SQUID) [5] or a flux qubit [6]. However, this standard method requires at least one wire to control one qubit, and the wiring of a large-scale system would be technically challenging in terms of packaging and reducing crosstalk. Furthermore, it cannot be applied for pulse control of a qubit in a 3D cavity [7–11] without adding wiring to the cavity, which weakens our ability to engineer the electromagnetic environment provided by the cavity.

In general, there are two types of qubit-resonator couplings: transverse and longitudinal [12]. The circuit QED architecture is a prime example of transverse coupling of a qubit to the displacement degree of freedom in a resonator. On the other hand, longitudinal coupling has recently been the focus of research for fast qubit readout [12–15] or coupling between two qubits [12,16–18]. Many efforts have been devoted to study the longitudinal coupling of a qubit to the displacement degree of freedom of a resonator [19–26]. However, the focus of this paper is longitudinal coupling of a qubit to the photon number degree of freedom of a resonator as we previously studied for the readout of a flux qubit [27–29] or ultrastrong coupling of a qubit and resonator [30].

Here, we present an alternative method in which the transition frequency of a flux qubit is controlled through its longitudinal coupling to the photon number degree of freedom in a resonator. A frequency-tunable resonator comprising a dc SQUID and capacitors works as a mediator between microwave photons in the resonator and the magnetic flux through the flux qubit because of the inductive coupling between the dc SQUID and qubit. Due to the longitudinal magnetic coupling, the flux qubit experiences an effective magnetic flux generated by the microwave photons in the resonator, and thus the transition frequency of the flux qubit can be controlled. By increasing the number of microwave photons in the resonator, the transition frequency of the flux qubit is successfully controlled up to ≈ 1.9 GHz.

In earlier works on the system with a flux qubit and a tunable resonator using a dc SQUID, the resonator was mainly used for reading out the qubit state [31,32]. Although the structure of our device is similar to them, the focus of this research is the control of the transition frequency of a flux qubit.

II. EXPERIMENT

A. Device and experimental setup

Figures 1(a) and 1(b), respectively, show an optical microscope image of the fabricated device and a scanning electron microscope image of the superconducting flux qubit [6,33] coupled to a frequency-tunable resonator containing the dc SQUID [34]. The lumped-element resonator consists of parallel plate capacitors (C), line inductors (L), and the dc SQUID [Fig. 1(c)] [35]. The flux qubit and the dc SQUID have shared edges [36], which ensures that the inductive coupling between them is strong enough. To excite the tunable resonator and flux qubit, we radiate the microwave pulse shown in Fig. 1(d) to them through the same on-chip microwave line (MW).

*hiraku.toida.ds@hco.ntt.co.jp

†Present address: Device Technology Research Institute, National Institute of Advanced Industrial Science and Technology, 1-1-1 Umezono, Tsukuba, Ibaraki 305-8568, Japan.

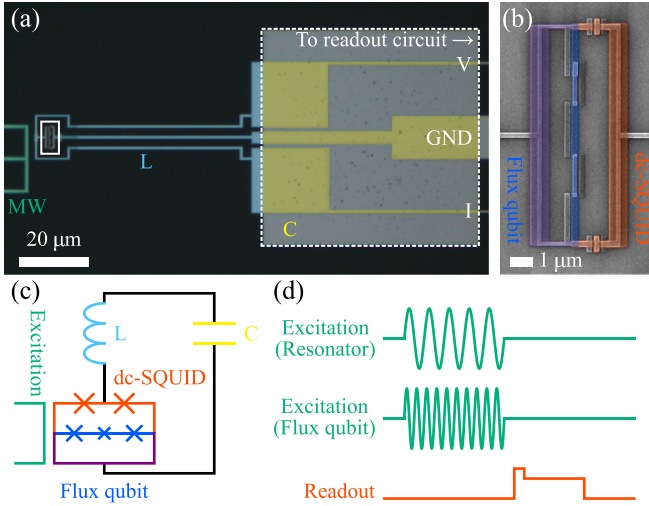


FIG. 1. (a) False color optical microscope image of the device. Microwave (MW) line (green), wire inductor L (sky blue), the top plate of parallel plate capacitors C (yellow), and bottom plate of parallel plate capacitors (white dotted area). The parallel plate capacitors consist of the top and bottom plates. After depositing the aluminum bottom plate, the film is oxidized to form a dielectric layer (AlO_x) between two plates. The dc SQUID is connected to a readout circuit for three-terminal measurements. The line indicated by V (I) is connected to the voltage (current) terminal. (b) False color scanning electron microscope image of the dc SQUID and flux qubit [white box in (a)]. The dc SQUID (red) and flux qubit (blue) share the edges of the loops (purple). (c) Equivalent circuit model of the device. The color scheme is the same as that in (a) and (b). The readout circuit for the dc SQUID is omitted. (d) Pulse sequence for the spectroscopy of the dc SQUID and/or flux qubit. Excitation signals are applied to the MW line, and a qubit readout pulse is sent to the dc SQUID.

The output signal of the microwave generator is attenuated by ≈ 73 dB in total, including the attenuation of ≈ 41 dB in the refrigerator. The resonator and the qubit states are read out by the switching probability of the dc SQUID [37]. The operating point of the tunable resonator and the flux qubit is controlled by applying an external magnetic field with a superconducting magnet. All the experiments were performed in a dilution refrigerator with a base temperature of about 25 mK.

B. Basic characteristic of the dc SQUID and the flux qubit

First, the properties of the tunable resonator and flux qubit are characterized independently. Figure 2(a) shows the spectrum of the tunable resonator as a function of the magnetic flux through the dc SQUID loop Φ_{SQ} . The resonance angular frequency of the tunable resonator ω_r can be controlled by Φ_{SQ} :

$$\omega_r(\Phi_{\text{SQ}}) = \omega_{\text{LC}} \frac{1}{\sqrt{1 + L_{\text{SQ}}(\Phi_{\text{SQ}})/L}}, \quad (1)$$

where $\omega_{\text{LC}} = (LC)^{-1/2}$ is the resonance angular frequency of the LC resonator without the dc SQUID, and L_{SQ} is the effective inductance of the dc SQUID controlled by Φ_{SQ} . The spectrum is missing around $\Phi_{\text{SQ}} \approx -4.0\Phi_0$, possibly because it is affected by an unwanted resonance around 4 GHz.

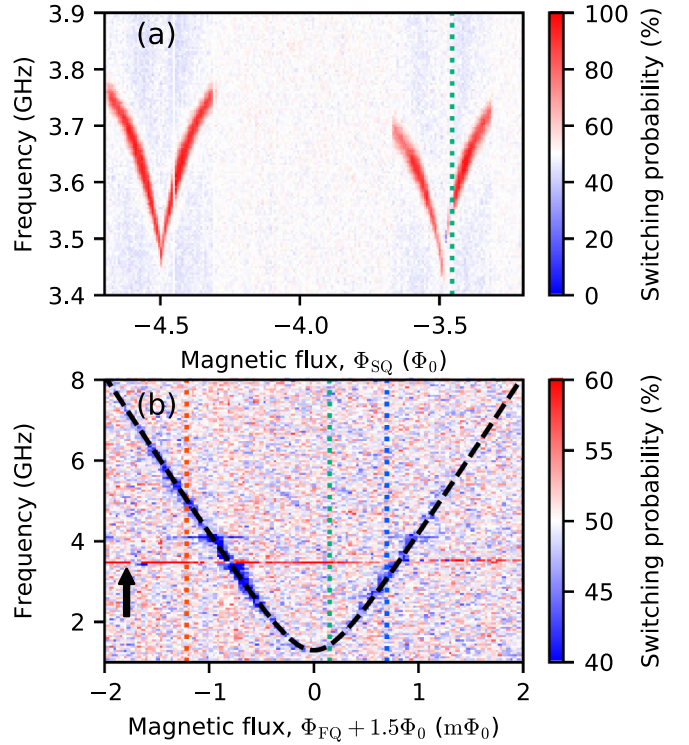


FIG. 2. (a) Spectrum of the frequency-tunable resonator as a function of applied flux Φ_{SQ} to the dc SQUID. The operating point of the flux qubit is indicated by the green dotted line. (b) Spectrum of the flux qubit as a function of applied flux Φ_{FQ} to the flux qubit loop. The resonance line indicated by the black arrow originates from the frequency-tunable resonator. Operating points used in two-tone spectroscopy are indicated by red, green, and blue dotted lines. The dashed line is the fit to the model [Eq. (2)].

The quality factor of the resonator is estimated from the linewidth of the peak to be ≈ 60 .

Figure 2(b) shows the spectrum of the flux qubit as a function of applied magnetic flux Φ_{FQ} to the flux qubit loop. The spectrum is reproduced by calculating the eigenenergy of the following Hamiltonian [38]:

$$\hat{H}_{\text{FQ}} = \frac{\Delta}{2} \hat{\sigma}_x + \frac{\varepsilon(\Phi_{\text{FQ}})}{2} \hat{\sigma}_z, \quad (2)$$

where $\hat{\sigma}_i$ ($i = x, z$) is the Pauli operator, Δ is the energy gap, $\varepsilon(\Phi_{\text{FQ}}) := 2I_p[\Phi_{\text{FQ}} - (N/2)\Phi_0]$ is the energy detuning with N being an odd integer, I_p is the persistent current, $\Phi_0 := h/2e$ is the magnetic flux quanta, h is the Planck's constant, and e is the elementary charge. Here, $N = -3$ is selected [39]. From the fitting to the flux qubit spectrum, the energy gap Δ/h is estimated to be 1.30 GHz. The persistent current is also extracted to be $I_p \approx 640$ nA from the slope of the spectrum. Estimated from other devices in the same batch, the flux qubit is expected to have a coherence time of the order of 100 ns at the optimal flux bias point. In the flux qubit spectrum, the horizontal straight line around 3.45 GHz indicated by the black arrow is the resonance of the tunable resonator. The frequency of the tunable resonator slightly changes in the qubit spectrum, because the flux range to tune the qubit is much narrower than that for tuning the resonator. However, it is important to note that the gradient

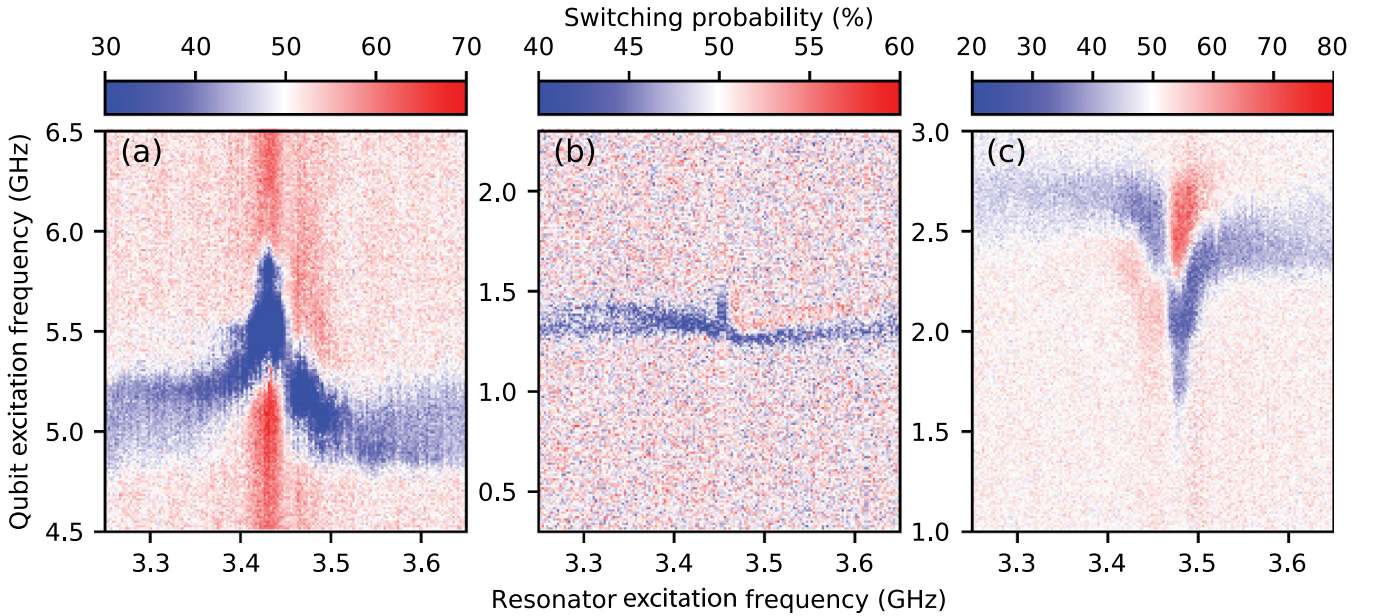


FIG. 3. Two-tone spectroscopy. Flux bias for the flux qubit is (a) -1.05 , (b) 0.13 , or (c) 0.60 $m\Phi_0$, respectively. These flux biases are indicated by the dotted lines in Fig. 2(b). Excitation power to the flux qubit and the resonator is the same for (a), (b), and (c). It is important to note that the peak or dip positions of the resonator are slightly different for (a)–(c) because of the small magnetic flux dependence of the resonator’s frequency.

of the tunable resonator spectrum is nonzero at the magnetic flux of the qubit operating point indicated by the green dotted line in Fig. 2(a). This is necessary for this scheme because the interaction between the resonator and qubit occurs because of the flux coupling between them. If the slope is nonzero, the resonator’s frequency is controlled by the magnetic flux generated by the qubit and vice versa.

C. Two-tone spectroscopy of the dc SQUID and the flux qubit

Next, two-tone spectroscopy was performed to control the transition frequency of the flux qubit through the excitation to the frequency-tunable resonator. In addition to a microwave tone for the qubit excitation (0.25 to 6.5 GHz), a secondary tone was applied to excite the frequency-tunable resonator (3.2 to 3.7 GHz). Figures 3 show the results of the two-tone spectroscopy. For this experiment, the operating point of the flux qubit was fixed at either -1.05 , 0.13 , or 0.60 $m\Phi_0$ indicated by red, green, and blue dotted lines, respectively, in Fig. 2(b). For these three experiments, the microwave excitation power to the resonator and flux qubit was fixed. If the flux bias is negative, the transition frequency of the flux qubit increases when the resonator is excited around 3.48 GHz [Fig. 3(a)]. On the other hand, if the flux bias is positive, the transition frequency of the flux qubit decreases [Fig. 3(c)]. It is also confirmed that the transition frequency changes little if near-zero flux bias is applied to the flux qubit [Fig. 3(b)].

D. Excitation power dependence of the frequency shift of the flux qubit

To investigate the frequency shift in more detail, the flux qubit spectrum was measured as a function of the excitation

power to the resonator as shown in Fig. 4(a). For this experiment, the flux bias for the flux qubit was set to almost zero (-0.067 $m\Phi_0$), and the microwave tone for the resonator excitation was fixed on resonance. As shown in Fig. 4(b), the transition frequency of the flux qubit increases linearly if the excitation power is large enough. It is important to note that the transition frequency converges to the energy gap of the flux qubit, Δ , with decreasing the excitation power. The linewidth of the flux qubit spectrum is also derived by fitting Fig. 4(a) to a Lorentzian function. As shown in Fig. 4(c), the linewidth of the flux qubit increases almost linearly with increasing the excitation power.

III. MODEL AND DISCUSSIONS

A. Photon number dependence of the qubit frequency

These experimental observations are explained by the total Hamiltonian of the system:

$$\hat{H} = \hat{H}_{\text{FQ}} + \hat{H}_{\text{r}} + \hat{H}_{\text{I}}, \quad (3)$$

$$\hat{H}_{\text{r}} = \hbar\omega_{\text{r}}^{(0)}(\Phi_{\text{SQ}})\hat{a}^\dagger\hat{a}, \quad (4)$$

where \hat{H}_{I} is the interaction Hamiltonian between the flux qubit and the tunable resonator, $\omega_{\text{r}}^{(0)}$ is the bare resonator frequency without perturbation from the flux qubit, and \hat{a} (\hat{a}^\dagger) is the annihilation (creation) operator for photons in the resonator.

Since there is a magnetic interaction between the dc SQUID and flux qubit, the resonance frequency of the tunable resonator is modified by the state of the flux qubit. The persistent current of the flux qubit, I_{p} , generates the magnetic flux through the dc SQUID, MI_{p} , where M is the mutual inductance between the dc SQUID and flux qubit. The change in the resonance frequency of the tunable resonator is

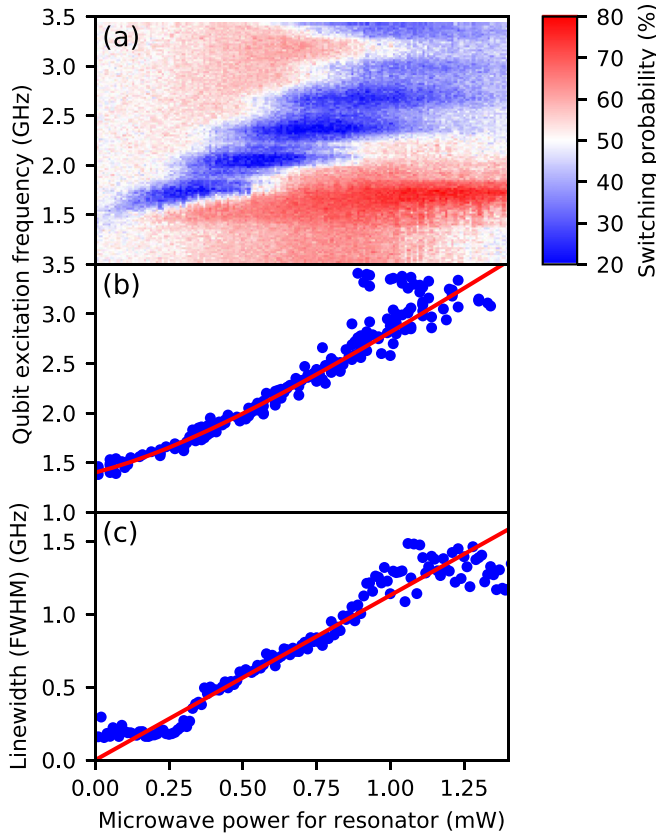


FIG. 4. Resonator excitation power dependence of the transition frequency of the flux qubit. The excitation frequency for the tunable resonator is fixed on resonance. (a) Qubit spectrum as a function of the excitation power of the resonator. The operation point of the flux qubit is fixed at $-0.067 \text{ m}\Phi_0$. The overall structure has a small ripple along the vertical axis due to the presence of parasitic resonances in the measurement setup. An additional peak appears near 3.5 GHz in the high power region because the frequency of the resonator is close. (b) Transition frequencies of the flux qubit extracted from (a). The solid line is the fit to the model [Eq. (8)] using the data below 0.8 mW. From the fit, the crossover power ($\Delta = |\varepsilon - g\bar{n}|$) is determined to be around 0.39 mW. Microwave power for the resonator was measured at the microwave generator. (c) Linewidth of the flux qubit extracted from (a). The solid line is a linear fit to the model [Eq. (11)] using the data between 0.4 mW and 0.8 mW.

approximated by $MI_p d\omega_r/d\Phi_{\text{SQ}}$. Thus, the interaction Hamiltonian is derived as follows:

$$\hat{H}_I = -\frac{g}{2}\hat{a}^\dagger\hat{a}|L\rangle\langle L| + \frac{g}{2}\hat{a}^\dagger\hat{a}|R\rangle\langle R| \quad (5)$$

$$= -\frac{g}{2}\hat{a}^\dagger\hat{a}\hat{\sigma}_z, \quad (6)$$

where $g := 2\hbar(d\omega_r/d\Phi_{\text{SQ}})MI_p$ is the coupling strength between the frequency-tunable resonator and flux qubit, and $|L\rangle$ ($|R\rangle$) is the eigenstate of the flux qubit corresponding to counterclockwise (clockwise) current. $\hat{\sigma}_z$ expresses the direction of the circulating current of the flux qubit. Equation (6) has a negative sign because the operation point of the flux qubit is near $N = -3$. From Eqs. (2)–(4) and (6),

the total Hamiltonian of the system is derived as follows:

$$\hat{H} = \frac{\Delta}{2}\hat{\sigma}_x + \frac{1}{2}(\varepsilon - g\hat{a}^\dagger\hat{a})\hat{\sigma}_z + \hbar\omega_r^{(0)}\hat{a}^\dagger\hat{a}. \quad (7)$$

From the eigenvalue of the Hamiltonian, the transition frequency of the flux qubit f_{FQ} is expressed as follows:

$$hf_{\text{FQ}} = \sqrt{(\varepsilon - g\bar{n})^2 + \Delta^2}, \quad (8)$$

where \bar{n} is the time averaged photon number in the resonator. This expression is linearized if the condition $|\varepsilon - g\bar{n}| \gg \Delta$ is satisfied:

$$hf_{\text{FQ}} \approx |\varepsilon - g\bar{n}|. \quad (9)$$

The model quantitatively explains the experimental results. In addition to energy detuning ε , the model has additional tunability of f_{FQ} stemming from the $g\bar{n}$ term. From Eq. (9), we can explain the dependence of the polarity of the shift of f_{FQ} on ε . If ε is negative [positive], f_{FQ} increases [decreases] as the photon number increases, which is observed in Figs. 3(a) and 3(c). To understand the phenomenon observed in Fig. 3(b), the equation before linearization [Eq. (8)] should be used, because the effect of the energy gap Δ cannot be ignored. In this case, the effect of the microwave photons in the resonator is not large compared to the cases of Figs. 3(a) and 3(c), which is consistent with the model.

Next, we investigate the shift of f_{FQ} as a function of the excitation power to the resonator [Fig. 4(b)]. Deviation from the linear trend is also observed in the low-power regime. This behavior is interpreted as the effect of the energy gap Δ as explained by Eq. (8).

Now, the coupling strength between the flux qubit and the dc SQUID g is estimated. From the device design parameters and individual experimental results for the flux qubit and resonator, the coupling strength is derived using the relationship $g = 2\hbar(d\omega_r/d\Phi_{\text{SQ}})MI_p$. Here, the mutual inductance between the flux qubit and dc SQUID, $M \approx 12.1 \text{ pH}$, is estimated by numerical simulation using FastHenry [40]. The persistent current of the flux qubit, I_p , is derived from the flux qubit spectrum [Fig. 2(b)] as previously shown. The slope of the resonator spectrum, $d\omega_r/d\Phi_{\text{SQ}} \approx 2\pi \times 2.1 \text{ GHz}/\Phi_0$, is directly derived from Fig. 2(a). By combining these values, the coupling strength is estimated to be $g \approx h \times 15.6 \text{ MHz}$.

It is important to emphasize the difference between the scheme presented here and a similar interaction of dispersive coupling between a qubit and resonator. In the circuit QED experiments in dispersive regime $\delta \gg g_c$ [δ (g_c) is the detuning (coupling strength) between the resonator and the qubit], the interaction Hamiltonian is approximated as $(g_c^2/\delta)\hat{a}^\dagger\hat{a}\hat{\sigma}_z$, and an ac Stark/Lamb shift is observed when we drive the resonator [41], although it is usually not intended to control the qubit frequency. In the case of dispersive coupling, the qubit frequency shift is relatively small because a large detuning δ suppresses the shift as $g_c^2/\delta \ll g_c$. Moreover, if we drive the resonator too strongly, the number of photons increases, which results in the violation of the dispersive approximation. On the other hand, there is no detuning dependence of the qubit frequency shift in our system. Our method also has the advantage that the increase in the number of photons does not change the form of the Hamiltonian in Eq. (7), although the

frequency shift is technically limited by the critical current of the dc SQUID. For these reasons, the qubit frequency can be controlled in a broad range without fundamental limitations. The sample used in the experiment showed the maximum frequency-tuning range of 1.9 GHz. This value is much larger than the typical case of circuit QED experiments in the order of ≈ 100 MHz [42–45]. In the experiment of a flux qubit inductively coupled to a linear resonator, the photon number dependent ac-Zeeman effect was observed [46]. This effect also changed the frequency of the flux qubit in the order of ≈ 100 MHz.

B. Photon number dependence of the dephasing rate

The effect of photon number fluctuations on the coherence property of the flux qubit is discussed here. Since the dephasing rate of a qubit is calculated using the interaction term containing the photon number operators $\hat{a}^\dagger \hat{a}$, two extreme cases are investigated to simplify the interaction term.

We can derive the interaction term for the case $\Delta \ll |\varepsilon - g\bar{n}|$ as follows:

$$\frac{1}{2}g\hat{a}^\dagger \hat{a} \hat{\sigma}_z. \quad (10)$$

It is important to note that this linear relationship to the photon number is the same form as the case of ac Stark shift [41]. The dephasing rate Γ_φ for this extreme case was calculated [41] as follows:

$$\Gamma_\varphi = 4\theta_0^2 \frac{\kappa}{2} \bar{n}, \quad (11)$$

$$\theta_0 = \frac{g}{\kappa}, \quad (12)$$

where κ is the relaxation rate of the tunable resonator.

If the condition $\Delta \gg |\varepsilon - g\bar{n}|$ is satisfied, we can approximate the interaction term as follows:

$$\frac{g^2}{4\Delta} (\hat{a}^\dagger \hat{a})^2 \hat{\sigma}_z. \quad (13)$$

Following the standard procedure to derive the dephasing rate caused by photon number fluctuation [41,47,48], the problem is translated into the calculation of correlation functions of creation and annihilation operators [49]. Finally, the dephasing factor $f_\varphi(t)$ is calculated as follows:

$$f_\varphi(t) = \exp\left(-\Gamma_\varphi t - \frac{\Sigma_\varphi^2 t^2}{2}\right), \quad (14)$$

$$\Gamma_\varphi = 4\theta_0^2 \frac{\kappa}{2} \bar{n}(\bar{n} + 1)(4\bar{n} + 1), \quad (15)$$

$$\Sigma_\varphi = \theta_0 \kappa \bar{n}, \quad (16)$$

$$\theta_0 = \frac{g^2}{2\Delta\kappa}. \quad (17)$$

See Appendix for detailed derivation. In our parameter range, the exponential decay is dominant. It is important to note that Eq. (15) has cubic dependence on the average photon number in the resonator. This may lead to a large dephasing rate of the qubit. However, the scaling factor θ_0 can be quite small due to the energy gap of the qubit. Thus, the dephasing rate can be negligible in a regime of small photon numbers. This is interpreted that the sensitivity of the transition frequency to

the photon number is small if $\Delta \gg |\varepsilon - g(\bar{n} + 1/2)|$ because the effect of the photon number is suppressed by the energy gap of the qubit as seen in Eq. (8).

In the experiment, a linear increase in the linewidth is observed in Fig. 4(c). This can be interpreted that the dephasing is caused by the photons in the resonator as shown in Eq. (11). In the low power regime, the deviation from the linear trend and saturation of the dephasing rate is observed. The former phenomenon is possibly caused by the crossover between the two regimes: with the qubit frequency dominated by Δ and with that dominated by $\varepsilon - g\bar{n}$, as seen in the qubit frequency shift [Fig. 4(b)]. The saturation value is an intrinsic dephasing rate induced by the factors other than photon number fluctuation.

IV. SUMMARY

In conclusion, by coupling a frequency-tunable resonator with a flux qubit, we demonstrated frequency control of the flux qubit, where the shift increases as the number of photons increases. Depending on the operation point of the flux qubit, either a positive or negative frequency shift is observed. The tuning range of the qubit frequency reaches 1.9 GHz. A model using longitudinal magnetic coupling between the flux qubit and frequency-tunable resonator quantitatively explains the experimental results with the coupling constant on the order of 10 MHz. Our method to control a flux qubit is applicable to c-shunt flux qubits [11,50,51], which have much better coherence properties compared to conventional flux qubits because they also have a relationship between the circulating current and the qubit state. The method would also be useful in implementing a large-scale quantum circuit with a smaller number of control lines or could provide further tunability to a flux qubit in a 3D cavity [11] without adding galvanic wiring into it.

ACKNOWLEDGMENTS

We thank Mao-Chuang Yeh, Anthony J. Leggett, and Hiroshi Yamaguchi for helpful discussions. This work was supported in part by MEXT Grant-in-Aid for Scientific Research on Innovative Areas ‘‘Science of hybrid quantum systems’’ (Grant No. 15H05867).

APPENDIX: DERIVATION OF EQ. (14)

Here, we derive the dephasing factor of the qubit for the case of $\Delta \gg |\varepsilon - g\bar{n}|$ using the similar procedure as the literature [41,48]. The interaction Hamiltonian for this limit is approximately expressed by the following term:

$$\frac{g^2}{4\Delta} \hat{n}^2(t) \hat{\sigma}_z, \quad (A1)$$

where $\hat{n}(t) = \hat{a}^\dagger(t) \hat{a}(t)$ is the photon number operator. The accumulated relative phase between the ground state and excited state during the period $[0, t]$ is derived by the following equation:

$$\hat{\varphi}(t) = \frac{g^2}{2\Delta} \int_0^t \hat{n}^2(t') dt'. \quad (A2)$$

The accumulated phase can be separated into two parts:

$$\hat{\varphi}(t) = \bar{\varphi}(t) + \delta\hat{\varphi}(t) \quad (\text{A3})$$

$$\bar{\varphi}(t) = \frac{g^2}{2\Delta} \bar{n}^2 t \quad (\text{A4})$$

$$\delta\hat{\varphi}(t) = \frac{g^2}{2\Delta} \int_0^t [\hat{n}^2(t') - \bar{n}^2] dt', \quad (\text{A5})$$

where $\bar{\varphi}(t)$ is the stationary phase evolution, and $\delta\hat{\varphi}(t)$ is the pure fluctuating part.

By using Eq. (A5), the dephasing factor $f_\varphi(t)$ can be expressed by the correlation function of photon number operators [48]:

$$f_\varphi(t) = \left\langle \exp \left(-i \int_0^t \delta\hat{\varphi}(t') dt' \right) \right\rangle \quad (\text{A6})$$

$$\cong \exp \left[-\frac{1}{2} \left(\frac{g^2}{2\Delta} \right)^2 \int_0^t \int_0^t C(t_1, t_2) dt_1 dt_2 \right], \quad (\text{A7})$$

$$C(t_1, t_2) = \langle [\hat{n}^2(t_1) - \bar{n}^2][\hat{n}^2(t_2) - \bar{n}^2] \rangle. \quad (\text{A8})$$

Since the resonator is coherently driven in our case, the annihilation operator is approximated by using canonical transformation:

$$\hat{a}(t) \cong \alpha(t) + \hat{d}(t), \quad (\text{A9})$$

where the coherent state $|\alpha\rangle$ satisfies $\hat{a}(t)|\alpha\rangle = \alpha(t)|\alpha\rangle$, thus $\hat{d}(t)$ is the vanishing operator for $|\alpha\rangle$.

Now, let us evaluate the correlation function

$$\langle \hat{a}^\dagger(t_1) \hat{a}(t_1) \hat{a}^\dagger(t_1) \hat{a}(t_1) \hat{a}^\dagger(t_2) \hat{a}(t_2) \hat{a}^\dagger(t_2) \hat{a}(t_2) \rangle. \quad (\text{A10})$$

By using Eq. (A9), the problem is translated into the calculation of correlation functions of creation and annihilation operators up to eight points. In general, Eq. (A10) is decomposed into $2^8 = 256$ terms of correlation functions. However, it can be proved that 242 terms vanish. More than three quarters of terms vanish by simply applying the relationship $\hat{d}^\dagger(t)|\alpha\rangle = 0$ or its conjugate. It is useful to use the commutation relation $[\hat{d}(t), \hat{d}^\dagger(t)] = 1$ to reduce the number of operators: j -point correlation functions can be translated into $(j - 2)$ -point ones.

By summing up the remaining 14 correlation functions containing an even number of creation and annihilation operators, and using the relationship [41]

$$\langle \hat{d}(t) \hat{d}^\dagger(0) \rangle \propto \exp \left(-\frac{\kappa}{2} |t| \right), \quad (\text{A11})$$

the dephasing factor is finally derived as follows:

$f_\varphi(t)$

$$\cong \exp \left[-\frac{1}{2} \left(\frac{g^2}{2\Delta} \right)^2 \bar{n}(\bar{n}+1)(4\bar{n}+1) \frac{4}{\kappa} t - \frac{1}{2} \left(\frac{g^2}{2\Delta} \right)^2 \bar{n}^2 t^2 \right]. \quad (\text{A12})$$

From this, the dephasing factor is derived to be Eq. (14).

-
- [1] F. Arute, K. Arya, R. Babbush, D. Bacon, J. C. Bardin, R. Barends, R. Biswas, S. Boixo, F. G. S. L. Brandao, D. A. Buell, B. Burkett, Y. Chen, Z. Chen, B. Chiaro, R. Collins, W. Courtney, A. Dunsworth, E. Farhi, B. Foxen, A. Fowler, C. Gidney, M. Giustina, R. Graff, K. Guerin, S. Habegger, M. P. Harrigan, M. J. Hartmann, A. Ho, M. Hoffmann, T. Huang, T. S. Humble, S. V. Isakov, E. Jeffrey, Z. Jiang, D. Kafri, K. Kechedzhi, J. Kelly, P. V. Klimov, S. Knysh, A. Korotkov, F. Kostritsa, D. Landhuis, M. Lindmark, E. Lucero, D. Lyakh, S. Mandrà, J. R. McClean, M. McEwen, A. Megrant, X. Mi, K. Michielsen, M. Mohseni, J. Mutus, O. Naaman, M. Neeley, C. Neill, M. Y. Niu, E. Ostby, A. Petukhov, J. C. Platt, C. Quintana, E. G. Rieffel, P. Roushan, N. C. Rubin, D. Sank, K. J. Satzinger, V. Smelyanskiy, K. J. Sung, M. D. Trevithick, A. Vainsencher, B. Villalonga, T. White, Z. J. Yao, P. Yeh, A. Zalcman, H. Neven, and J. M. Martinis, *Nature (London)* **574**, 505 (2019).
- [2] A. D. Córcoles, A. Kandala, A. Javadi-Abhari, D. T. McClure, A. W. Cross, K. Temme, P. D. Nation, M. Steffen, and J. M. Gambetta, *Proc. IEEE* **108**, 1 (2019).
- [3] J. S. Otterbach, R. Manenti, N. Alidoust, A. Bestwick, M. Block, B. Bloom, S. Caldwell, N. Didier, E. S. Fried, S. Hong, P. Karalekas, C. B. Osborn, A. Papageorge, E. C. Peterson, G. Prawiroatmodjo, N. Rubin, C. A. Ryan, D. Scarabelli, M. Scheer, E. A. Sete, P. Sivarajah, R. S. Smith, A. Staley, N. Tezak, W. J. Zeng, A. Hudson, B. R. Johnson, M. Reagor, M. P. da Silva, and C. Rigetti, [arXiv:1712.05771](https://arxiv.org/abs/1712.05771).
- [4] M. Gong, M.-C. Chen, Y. Zheng, S. Wang, C. Zha, H. Deng, Z. Yan, H. Rong, Y. Wu, S. Li, F. Chen, Y. Zhao, F. Liang, J. Lin, Y. Xu, C. Guo, L. Sun, A. D. Castellano, H. Wang, C. Peng, C.-Y. Lu, X. Zhu, and J.-W. Pan, *Phys. Rev. Lett.* **122**, 110501 (2019).
- [5] Y. Nakamura, Y. A. Pashkin, and J. S. Tsai, *Nature (London)* **398**, 786 (1999).
- [6] J. E. Mooij, T. P. Orlando, L. Levitov, L. Tian, C. H. van der Wal, and S. Lloyd, *Science* **285**, 1036 (1999).
- [7] H. Paik, D. I. Schuster, L. S. Bishop, G. Kirchmair, G. Catelani, A. P. Sears, B. R. Johnson, M. J. Reagor, L. Frunzio, L. I. Glazman, S. M. Girvin, M. H. Devoret, and R. J. Schoelkopf, *Phys. Rev. Lett.* **107**, 240501 (2011).
- [8] C. Rigetti, J. M. Gambetta, S. Poletto, B. L. T. Plourde, J. M. Chow, A. D. Córcoles, J. A. Smolin, S. T. Merkel, J. R. Rozen, G. A. Keefe, M. B. Rothwell, M. B. Ketchen, and M. Steffen, *Phys. Rev. B* **86**, 100506(R) (2012).
- [9] M. Stern, G. Catelani, Y. Kubo, C. Grezes, A. Bienfait, D. Vion, D. Esteve, and P. Bertet, *Phys. Rev. Lett.* **113**, 123601 (2014).
- [10] M. Reagor, W. Pfaff, C. Axline, R. W. Heeres, N. Ofek, K. Sliwa, E. Holland, C. Wang, J. Blumoff, K. Chou, M. J. Hatridge, L. Frunzio, M. H. Devoret, L. Jiang, and R. J. Schoelkopf, *Phys. Rev. B* **94**, 014506 (2016).
- [11] L. V. Abdurakhimov, I. Mahboob, H. Toida, K. Kakuyanagi, and S. Saito, *Appl. Phys. Lett.* **115**, 262601 (2019).
- [12] P.-M. Billangeon, J. S. Tsai, and Y. Nakamura, *Phys. Rev. B* **91**, 094517 (2015).
- [13] N. Didier, J. Bourassa, and A. Blais, *Phys. Rev. Lett.* **115**, 203601 (2015).

- [14] S. Touzard, A. Kou, N. E. Frattini, V. V. Sivak, S. Puri, A. Grimm, L. Frunzio, S. Shankar, and M. H. Devoret, *Phys. Rev. Lett.* **122**, 080502 (2019).
- [15] J. Ikonen, J. Goetz, J. Ilves, A. Keränen, A. M. Gunyho, M. Partanen, K. Y. Tan, D. Hazra, L. Grönberg, V. Vesterinen, S. Simbierowicz, J. Hassel, and M. Möttönen, *Phys. Rev. Lett.* **122**, 080503 (2019).
- [16] B. Royer, A. L. Grimsmo, N. Didier, and A. Blais, *Quantum* **1**, 11 (2017).
- [17] M. R. Geller, E. Donate, Y. Chen, M. T. Fang, N. Leung, C. Neill, P. Roushan, and J. M. Martinis, *Phys. Rev. A* **92**, 012320 (2015).
- [18] S. J. Weber, G. O. Samach, D. Hover, S. Gustavsson, D. K. Kim, A. Melville, D. Rosenberg, A. P. Sears, F. Yan, J. L. Yoder, W. D. Oliver, and A. J. Kerman, *Phys. Rev. Appl.* **8**, 014004 (2017).
- [19] Y. xi Liu, C.-X. Yang, H.-C. Sun, and X.-B. Wang, *New J. Phys.* **16**, 015031 (2014).
- [20] Y.-J. Zhao, Y.-L. Liu, Y.-x. Liu, and F. Nori, *Phys. Rev. A* **91**, 053820 (2015).
- [21] S. Richer and D. DiVincenzo, *Phys. Rev. B* **93**, 134501 (2016).
- [22] X. Wang, H.-r. Li, D.-x. Chen, W.-x. Liu, and F.-l. Li, *Opt. Commun.* **366**, 321 (2016).
- [23] X. Wang, A. Miranowicz, H.-R. Li, and F. Nori, *Phys. Rev. A* **94**, 053858 (2016).
- [24] X. Gu, A. F. Kockum, A. Miranowicz, Y.-x. Liu, and F. Nori, *Phys. Rep.* **718**, 1 (2017).
- [25] R. Stassi and F. Nori, *Phys. Rev. A* **97**, 033823 (2018).
- [26] X. Wang, A. Miranowicz, and F. Nori, *Phys. Rev. Appl.* **12**, 064037 (2019).
- [27] H. Nakano, S. Saito, K. Semba, and H. Takayanagi, *Phys. Rev. Lett.* **102**, 257003 (2009).
- [28] K. Kakuyanagi, S. Kagei, R. Koibuchi, S. Saito, A. Lupaşcu, K. Semba, and H. Nakano, *New J. Phys.* **15**, 043028 (2013).
- [29] K. Kakuyanagi, T. Baba, Y. Matsuzaki, H. Nakano, S. Saito, and K. Semba, *New J. Phys.* **17**, 063035 (2015).
- [30] S. Endo, Y. Matsuzaki, K. Kakuyanagi, S. Saito, N. Lambert, and F. Nori, *Sci. Rep.* **10**, 1751 (2020).
- [31] A. Lupaşcu, C. J. M. Verwijs, R. N. Schouten, C. J. P. M. Harmans, and J. E. Mooij, *Phys. Rev. Lett.* **93**, 177006 (2004).
- [32] A. Lupaşcu, E. F. C. Driessen, L. Roschier, C. J. P. M. Harmans, and J. E. Mooij, *Phys. Rev. Lett.* **96**, 127003 (2006).
- [33] T. P. Orlando, J. E. Mooij, L. Tian, C. H. van der Wal, L. S. Levitov, S. Lloyd, and J. J. Mazo, *Phys. Rev. B* **60**, 15398 (1999).
- [34] J. Johansson, S. Saito, T. Meno, H. Nakano, M. Ueda, K. Semba, and H. Takayanagi, *Phys. Rev. Lett.* **96**, 127006 (2006).
- [35] J. Y. Mutus, T. C. White, E. Jeffrey, D. Sank, R. Barends, J. Bochmann, Y. Chen, Z. Chen, B. Chiaro, A. Dunsworth, J. Kelly, A. Megrant, C. Neill, P. J. J. O'Malley, P. Roushan, A. Vainsencher, J. Wenner, I. Siddiqi, R. Vijay, A. N. Cleland, and J. M. Martinis, *Appl. Phys. Lett.* **103**, 122602 (2013).
- [36] I. Chiorescu, Y. Nakamura, C. J. P. M. Harmans, and J. E. Mooij, *Science* **299**, 1869 (2003).
- [37] F. Deppe, M. Mariantoni, E. P. Menzel, S. Saito, K. Kakuyanagi, H. Tanaka, T. Meno, K. Semba, H. Takayanagi, and R. Gross, *Phys. Rev. B* **76**, 214503 (2007).
- [38] C. H. van der Wal, A. C. J. ter Haar, F. K. Wilhelm, R. N. Schouten, C. J. P. M. Harmans, T. P. Orlando, S. Lloyd, and J. E. Mooij, *Science* **290**, 773 (2000).
- [39] X. Zhu, A. Kemp, S. Saito, and K. Semba, *Appl. Phys. Lett.* **97**, 102503 (2010).
- [40] M. Kamon, M. J. Tsuk, and J. White, in *Proceedings of the 30th International Design Automation Conference, DAC '93* (Association for Computing Machinery, New York, 1993), pp. 678–683.
- [41] A. Blais, R.-S. Huang, A. Wallraff, S. M. Girvin, and R. J. Schoelkopf, *Phys. Rev. A* **69**, 062320 (2004).
- [42] D. I. Schuster, A. Wallraff, A. Blais, L. Frunzio, R.-S. Huang, J. Majer, S. M. Girvin, and R. J. Schoelkopf, *Phys. Rev. Lett.* **94**, 123602 (2005).
- [43] D. I. Schuster, A. Wallraff, A. Blais, L. Frunzio, R.-S. Huang, J. Majer, S. M. Girvin, and R. J. Schoelkopf, *Phys. Rev. Lett.* **98**, 049902(E) (2007).
- [44] D. I. Schuster, A. A. Houck, J. A. Schreier, A. Wallraff, J. M. Gambetta, A. Blais, L. Frunzio, J. Majer, B. Johnson, M. H. Devoret, S. M. Girvin, and R. J. Schoelkopf, *Nature (London)* **445**, 515 (2007).
- [45] F. R. Ong, M. Boissonneault, F. Mallet, A. Palacios-Laloy, A. Dewes, A. C. Doherty, A. Blais, P. Bertet, D. Vion, and D. Esteve, *Phys. Rev. Lett.* **106**, 167002 (2011).
- [46] A. A. Abdumalikov, O. Astafiev, Y. Nakamura, Y. A. Pashkin, and J. S. Tsai, *Phys. Rev. B* **78**, 180502(R) (2008).
- [47] P. Bertet, I. Chiorescu, G. Burkard, K. Semba, C. J. P. M. Harmans, D. P. DiVincenzo, and J. E. Mooij, *Phys. Rev. Lett.* **95**, 257002 (2005).
- [48] P. Bertet, I. Chiorescu, C. J. P. M. Harmans, and J. E. Mooij, *arXiv:cond-mat/0507290*.
- [49] L. Mandel and E. Wolf, *Optical Coherence and Quantum Optics* (Cambridge University Press, Cambridge, 1995).
- [50] F. Yan, S. Gustavsson, A. Kamal, J. Birenbaum, A. P. Sears, D. Hover, T. J. Gudmundsen, D. Rosenberg, G. Samach, S. Weber, J. L. Yoder, T. P. Orlando, J. Clarke, A. J. Kerman, and W. D. Oliver, *Nat. Commun.* **7**, 12964 (2016).
- [51] F. Yan, D. Campbell, P. Krantz, M. Kjaergaard, D. Kim, J. L. Yoder, D. Hover, A. Sears, A. J. Kerman, T. P. Orlando, S. Gustavsson, and W. D. Oliver, *Phys. Rev. Lett.* **120**, 260504 (2018).